MATERIALS SCIENCE

Electromagnetic interference shielding with 2D transition metal carbides (MXenes)

Faisal Shahzad,[1,2]* Mohamed Alhabeb,[3]* Christine B. Hatter,[3]* Babak Anasori,[3] Soon Man Hong,[1] Chong Min Koo,[1,2]† Yury Gogotsi[3]†

Materials with good flexibility and high conductivity that can provide electromagnetic interference (EMI) shielding with minimal thickness are highly desirable, especially if they can be easily processed into films. Two-dimensional metal carbides and nitrides, known as MXenes, combine metallic conductivity and hydrophilic surfaces. Here, we demonstrate the potential of several MXenes and their polymer composites for EMI shielding. A 45-micrometer-thick $Ti_3C_2T_x$ film exhibited EMI shielding effectiveness of 92 decibels (>50 decibels for a 2.5-micrometer film), which is the highest among synthetic materials of comparable thickness produced to date. This performance originates from the excellent electrical conductivity of $Ti_3C_2T_x$ films (4600 Siemens per centimeter) and multiple internal reflections from $Ti_3C_2T_x$ flakes in free-standing films. The mechanical flexibility and easy coating capability offered by MXenes and their composites enable them to shield surfaces of any shape while providing high EMI shielding efficiency.

Electronic devices are getting smarter, being made smaller, and growing in number every day. Any electronic device that transmits, distributes, or uses electrical energy creates electromagnetic interference (EMI) that has detrimental impacts on device performance and the surrounding environment. As electronics and their components operate at faster speeds and smaller size, a substantial increase in EMI results, which can lead to malfunctioning and degradation of electronics (*1*–*4*). This increase in electromagnetic pollution can also affect human health, as well as the surrounding environment, if no shielding is provided (*5*).

An effective EMI shielding material must both reduce undesirable emissions and protect the component from stray external signals. The primary function of EMI shielding is to reflect radiation using charge carriers that interact directly with the electromagnetic (EM) fields (*6*). As a result, shielding materials need to be electrically conductive. However, conductivity is not the only requirement. The secondary mechanism of EMI shielding requires absorption of EM radiation due to the material's electric and/or magnetic dipoles interacting with the radiation. High electrical conductivity is the primary factor determining reflectivity and absorption characteristics of the shield (*7*). However, a third mechanism accounting for multiple internal reflections is less studied but contributes substantially to EMI shielding effectiveness. These internal reflections arise from scattering centers and interfaces or defect sites within the shielding material, resulting in scattering and then absorption of EM waves (EMWs) (*1*, *8*, *9*).

Previously, metal shrouds were the material of choice to combat EMI interference (*1*–*4*) (*6*–*10*), but with smaller devices and components, adding additional weight coupled with susceptibility to corrosion makes metals less desirable (*8*). Lightweight, low-cost, high-strength and easy-to-fabricate shielding materials are therefore needed. Polymer-matrix composites with embedded conductive fillers have become a popular alternative for EMI shielding because of high processability and low densities (*10*). Carbon-based fillers, particularly carbon nanotubes and graphene in combination with magnetic constituents, have attracted much interest in recent years (*11*), but no breakthrough has been reported thus far. New EMI shielding materials that can exceed the requirements of next-generation portable equipment and wearable devices are strongly needed.

MXenes are a unique family of two-dimensional (2D) transition metal carbides and/or nitrides with the formula $M_{n+1}X_nT_x$, where M is an early transition metal (e.g., Ti, Zr, V, Nb, Ta, or Mo) and X is carbon and/or nitrogen. Owing to the aqueous medium used during synthesis, MXene flakes are terminated with surface moieties (T_x), such as a mixture of –OH, =O, and –F (*12*). Metallic conductivity and good mechanical properties coupled with hydrophilicity make MXenes a good candidate for use in polymer composites (*12*) and energy storage devices (*13*) as they can intercalate organic molecules and ions. About 20 different MXenes have already been reported (*12*, *14*, *15*). Thus far, the most commonly studied MXene, $Ti_3C_2T_x$, has been incorporated into different polymer matrices such as ultrahigh–molecular weight polyethylene (UMWPE), polypyrrole (PPy), and polyvinyl alcohol (PVA). The MXene-polymer composites exhibited improved tensile strength, but good conductivity was maintained at low polymer loadings (*16*, *17*). A previous study incorporating a naturally occurring polymer, sodium alginate (SA), as a binder for Li-ion batteries (*18*) showed retention of electrode conductivity, the primary component for EMI shielding. SA is a linear polysaccharide copolymer derived from seaweed. Natural biomaterials, like SA, are potentially ideal candidates for polymeric matrices because they are abundant, do not harm the environment, and are mechanically robust. SA has oxygen-containing functional groups (–OH, –COO, and =O), which can potentially facilitate the formation of hydrogen bonding with the termination

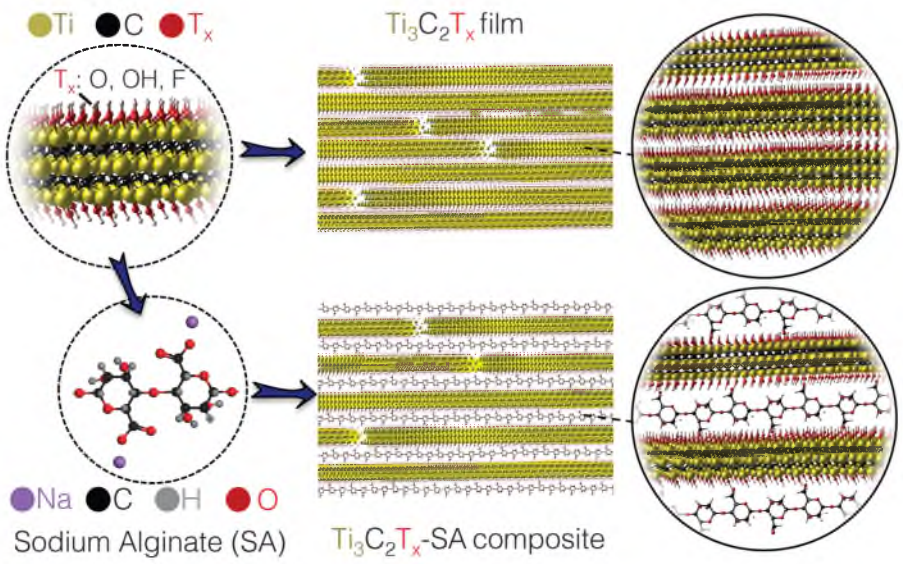

Fig. 1. Schematic of $Ti_3C_2T_x$ and $Ti_3C_2T_x$-SA composite films.

[1]Materials Architecturing Research Center, Korea Institute of Science and Technology, 5, Hwarang-ro 14-gil, Seongbuk-gu, Seoul 02792, Republic of Korea. [2]Nanomaterials Science and Engineering, University of Science and Technology, 217, Gajung-ro, Yuseong-gu, Daejeon 34113, Republic of Korea. [3]Department of Materials Science and Engineering, and A. J. Drexel Nanomaterials Institute, Drexel University, 3141 Chestnut Street, Philadelphia, PA 19104, USA.
*These authors contributed equally to this work. †Corresponding author. Email: gogotsi@drexel.edu (Y.G.); koo@kist.re.kr (C.M.K.)

groups of MXenes. To date, no MXene-SA composites have been reported in the literature.

Here we report highly flexible MXene films ($Ti_3C_2T_x$, $Mo_2TiC_2T_x$, and $Mo_2Ti_2C_3T_x$) and nacre-like MXene–polymer composite films ($Ti_3C_2T_x$-SA) with excellent EMI shielding performance. All free-standing films were made by vacuum-assisted filtration starting from colloidal solutions of pure MXenes or its composites (fig. S1). The schematic representation of the layered structure for MXene-SA composites is displayed in Fig. 1. Both $Ti_3C_2T_x$ film (45 μm) and $Ti_3C_2T_x$-SA [8 μm, 10 weight % (wt %) SA], in particular, exhibit extraordinary EMI shielding effectiveness (SE) of 92 and 57 dB, respectively. These MXene films have additional advantages such as high conductivity, easy processing, relatively low density, and mechanical flexibility. To our knowledge, this is the highest EMI SE performance reported for synthetic materials of similar thickness and is comparable to the EMI SE performance of pure metals. This finding paves the way for the development of a large family of EMI shielding materials.

The scanning electron microscopy (SEM) image of a $Ti_3C_2T_x$ MXene flake (size range from 1 to 5 μm) on an alumina filter is shown in Fig. 2A, in which the MXene flake is almost transparent to the electron beam. The cross-sectional SEM images of the 50 wt % $Ti_3C_2T_x$-SA, and pristine $Ti_3C_2T_x$ are shown in Fig. 2, B and C, respectively. In all composite loadings, the nacre-like layered stacking of the $Ti_3C_2T_x$ remains; similar to that of the pristine $Ti_3C_2T_x$ films. This characteristic is also confirmed by the presence of the $Ti_3C_2T_x$ (002) peak in all the $Ti_3C_2T_x$-SA x-ray diffraction (XRD) patterns (Fig. 2D). The intensity of all the (00*l*) $Ti_3C_2T_x$ peaks in the composite samples is decreased compared to that of the pristine $Ti_3C_2T_x$, owing to the presence of SA between the layers. The introduction of SA adds disorder in stacking and separates MXene flakes. Additionally, a new peak around ~4.4° appears after the addition of SA, and its intensity increases with SA content (compare the top two patterns in Fig. 2D). This peak corresponds to a $Ti_3C_2T_x$ interlayer spacing of ~10 Å, a result of SA presence between MXene layers. In the case of 30 wt % $Ti_3C_2T_x$-SA, the broad (002) peak is between ≤4.4° and 6.5°, which is due to the variable interlayer spacings between MXene layers, ranging from >10 to 3.5 Å. This shows that although SA molecules are intercalated between MXene layers, the latter still retains the ordered layered structure.

Cross-sectional transmission electron microscopy (TEM) images of the $Ti_3C_2T_x$-SA composite films confirm the intercalation of SA layers in-between MXene flakes. At higher $Ti_3C_2T_x$ contents, mostly stacks of $Ti_3C_2T_x$ flakes, with some individual flakes separated with SA, are observed (Fig. 2E). This feature could be due to MXene restacking during filtration. At lower $Ti_3C_2T_x$ concentrations, more individual $Ti_3C_2T_x$ flakes are separated with SA, and a variety of different interlayer spacings are present (Fig. 2F). However, some MXene restacking does occur even at lower MXene concentrations (fig. S2). This combination of different spacing between layers can explain the very broad range of the (002) peaks observed in 30 wt % $Ti_3C_2T_x$-SA XRD patterns from ≤4.4° to 6.5°.

Materials with large electrical conductivity are typically needed to obtain high EMI SE values. Figure 3A presents the electrical conductivity of three different types of MXenes. A higher electrical conductivity in $Mo_2Ti_2C_3T_x$ was observed compared to $Mo_2TiC_2T_x$, which is in agreement with previously reported results (*19*). $Ti_3C_2T_x$ films showed the highest electrical conductivity among the studied samples, reaching 4600 S cm^{-1}. Such excellent electrical conductivity arises from the high electron density of states near the Fermi level [$N(E_f)$] as predicted from density functional theory (DFT) (*20*), making this MXene metallic in nature. By contrast, $Mo_2TiC_2T_x$ and $Mo_2Ti_2C_3T_x$ exhibited lower electrical conductivity values of 119.7 and 297.0 S cm^{-1}, respectively, and semiconductor-like temperature dependence of conductivity (*15*, *19*).

Electrical conductivities of $Ti_3C_2T_x$-SA polymer composites are plotted in Fig. 3B. With the addition of only 10 wt % $Ti_3C_2T_x$, the conductivity of SA polymer rises to 0.5 S cm^{-1}. The large aspect ratio of $Ti_3C_2T_x$ flakes likely provides a percolation network at low filler loading, thereby increasing electrical conductivity of the composite sample. As filler content is increased, electrical conductivity increases and reaches 3000 S cm^{-1} for the 90 wt % $Ti_3C_2T_x$-SA composite.

To explore the EMI shielding properties of MXenes, we compared three MXene film compositions with an average thickness of ~ 2.5 μm in Fig. 3C. EMI SE is directly proportional to electrical conductivity (eq. 2, supplementary materials). Consequently, $Ti_3C_2T_x$, with the best electrical conductivity, gives the highest EMI SE among the studied MXenes. Because thickness plays a crucial role in EMI SE of any material, EMI SE can be improved simply by increasing the thickness. To investigate this effect, we measured the EMI SE of six $Ti_3C_2T_x$ films with different thicknesses in Fig. 3D. The highest EMI SE value, 92 dB, was recorded for a 45-μm-thick film, enough to block 99.99999994% of incident radiation with only 0.00000006% transmission (table S1). Experimental results of a $Ti_3C_2T_x$ film in the X-band are comparable to the theoretically calculated values using eq. 2 (supplementary materials) that predicts high EMI SE values of $Ti_3C_2T_x$ films at lower frequencies, as well (see fig. S3A). Experimental measurements on a laminated spray-coated 4-μm-thick film (fig. S1) confirmed the prediction, showing similar EMI SE values at high and low frequencies. Thus, MXene films maintain excellent EMI SE shielding capability over a broad frequency range (fig. S3B).

In general, adequate shielding can be achieved by using thick conventional materials; however, material consumption and weight put such materials at a disadvantage for use in aerospace and

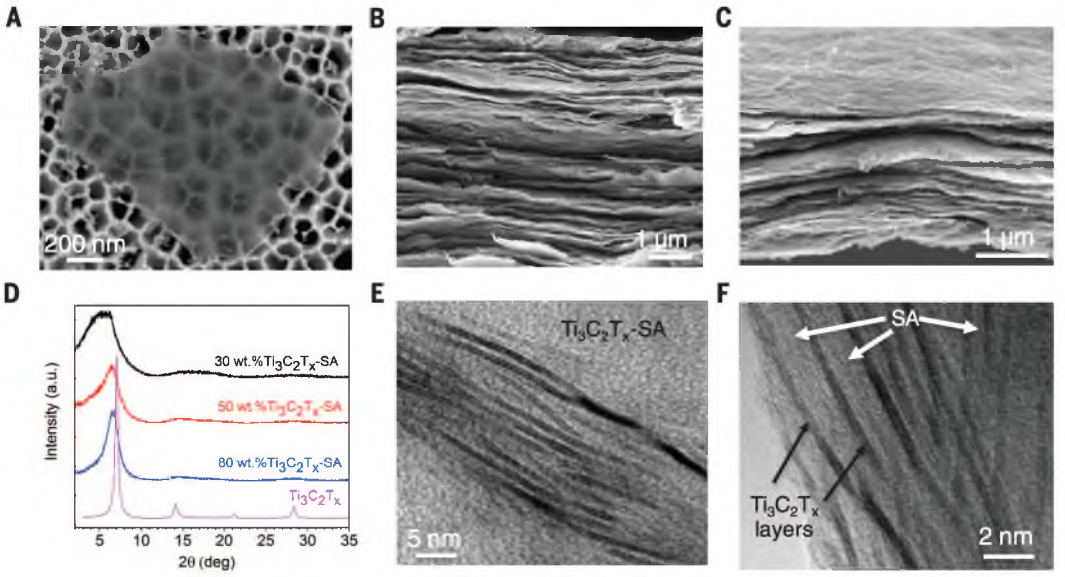

Fig. 2. Morphological and structural characterization of $Ti_3C_2T_x$ and $Ti_3C_2T_x$-SA composites. (**A**) SEM image of a $Ti_3C_2T_x$ flake on a filter. (**B** and **C**) SEM images of (B) 50 wt % $Ti_3C_2T_x$-SA composite and (C) pure $Ti_3C_2T_x$. (**D**) XRD patterns of pristine $Ti_3C_2T_x$ and its composite with SA at different loadings. (**E** and **F**) TEM images of 80 and 30 wt % $Ti_3C_2T_x$-SA composite films, respectively.

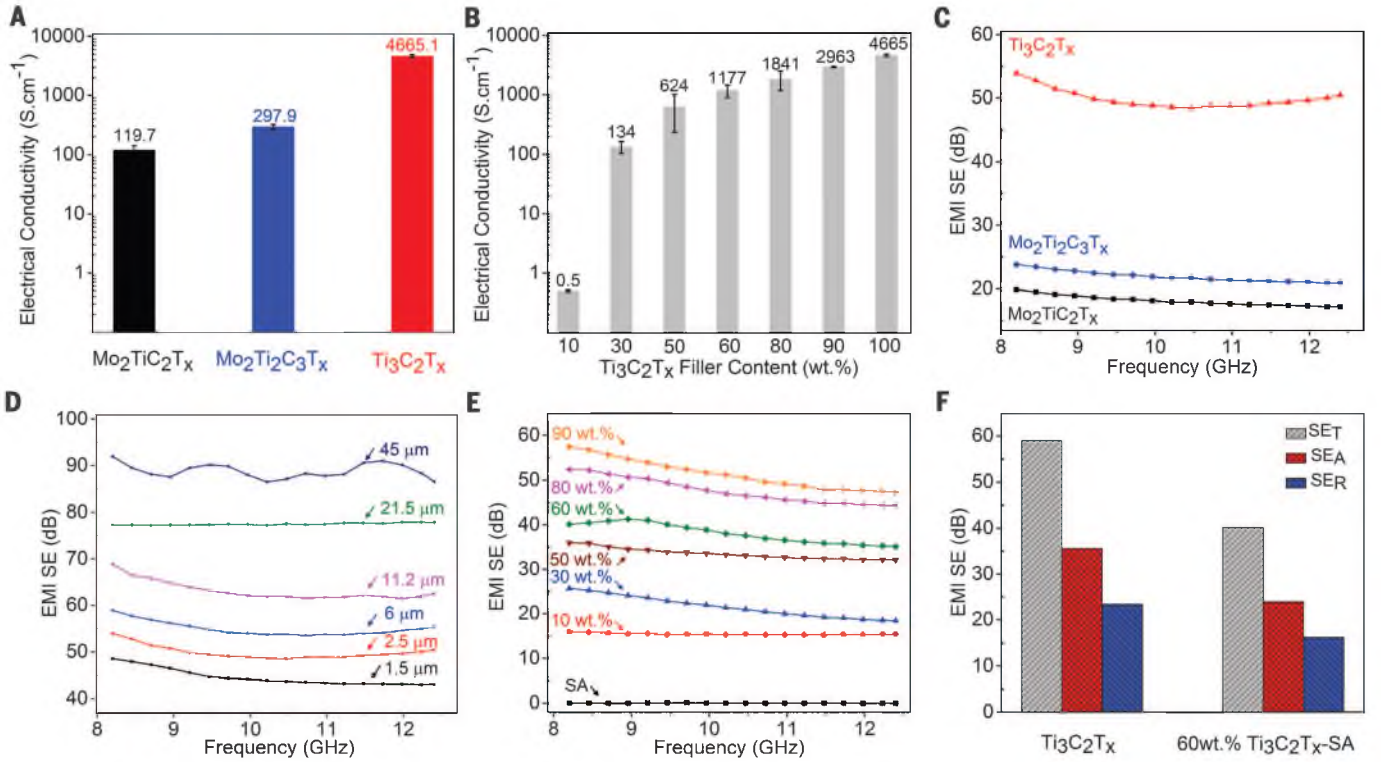

Fig. 3. Electrical conductivity and EMI SE of MXene and MXene composites. (**A**) Electrical conductivity of $Mo_2TiC_2T_x$, $Mo_2Ti_2C_3T_x$, and $Ti_3C_2T_x$. (**B**) Electrical conductivity of $Ti_3C_2T_x$-SA composites. Filler content varies from 10 to 90 wt % $Ti_3C_2T_x$ in SA matrix. (**C**) EMI SE of $Mo_2TiC_2T_x$, $Mo_2Ti_2C_3T_x$, $Ti_3C_2T_x$ at a thickness of ~2.5 μm. (**D**) EMI SE of $Ti_3C_2T_x$ at different thicknesses. (**E**) EMI SE of $Ti_3C_2T_x$-SA composites at a thickness of 8 to 9 μm. (**F**) Total EMI SE (EMI SE_T) and its absorption (SE_A) and reflection (SE_R) mechanism in $Ti_3C_2T_x$ and 60 wt % $Ti_3C_2T_x$-SA samples at 8.2 GHz.

telecommunication applications. Therefore, it is important to achieve high EMI SE values with relatively thin films. As discussed above, to further improve MXenes mechanical properties and environmental stability, and to reduce their weight, we can embed them in polymer matrices. As an example, we investigated the $Ti_3C_2T_x$-SA composites for EMI shielding. Here, the thickness of composite films was fixed between 8 and 9 μm. With increasing MXene content, EMI SE increased, to a maximum of 57 dB for the 90 wt % $Ti_3C_2T_x$-SA sample (Fig. 3E). To obtain a clearer picture, we plotted the influence of filler content on EMI SE at a constant frequency of 8.2 GHz (see fig. S4). Shielding mechanism from absorption (SE_A) and reflection (SE_R) in the $Ti_3C_2T_x$ (6 μm) and 60 wt % $Ti_3C_2T_x$-SA (~8 μm) films were plotted in Fig. 3F at 8.2 GHz. Shielding due to absorption was the dominant mechanism, rather than reflection in pristine MXene and its composites.

A comprehensive literature review of previously studied materials for EMI SE (table S2) clearly indicates that MXenes and their composites are the best EMI shielding materials known to date. So far, most research has focused on graphene (*11*, *21*, *22*), carbon nanotubes (*23*), iron oxides (*24*), ferrites (*25*), iron-aluminum-silicon alloys (*26*), and metallic-based filler (*27*) polymer composites. However, to satisfy the common commercial EMI shielding requirements (above 30 dB) (*2*), large thicknesses, usually more than 1 mm, are needed. Ultrathin MXene films clearly outperform all of the known synthetic materials and rank at the top of the comparison chart (Fig. 4A).

Recently, the concept of foam structures has gained tremendous interest as a way to reduce the density of shielding materials. Lightweight materials are a necessity for aerospace applications; therefore, some metals (such as copper and silver) that possess high EMI SE values are less useful (*1*, *28*–*30*). When considering a material's density, specific EMI shielding effectiveness (SSE) is used as a criterion to evaluate different materials. However, SSE alone is not a sufficient parameter for understanding overall effectiveness, as a higher SSE can simply be achieved at a larger thickness, which directly increases the weight of the final product. Therefore, a more realistic parameter is to divide SSE by the material thickness (SSE/*t*) (*27*, *31*). Such a parameter is highly valuable for determining the effectiveness of a material by incorporating three important factors: EMI SE, density, and thickness. Interestingly, SSE/*t* values for MXene and MXene-SA composites are much higher than those for other materials of different categories (table S3). As a representative example, a 90 wt % $Ti_3C_2T_x$-SA composite sample gives a SSE/*t* of 30,830 dB cm^2 g^{-1}, which is several times higher than those of the other materials studied thus far (fig. S5). This finding is notable because several commercial requirements for an EMI shielding product are engrained in a single material, such as high EMI SE (57 dB), low density (2.31 g cm^{-3}), small thickness (8 μm, reducing net weight and volume), oxidation resistance (due to polymer binder), high flexibility (a feature of 2D films), and simple processing (mixing and filtration or spray-coating). Going a step further, $Ti_3C_2T_x$ and $Ti_3C_2T_x$-SA composites were compared with pure aluminum (8 μm) and copper (10 μm) foils (fig. S6). $Ti_3C_2T_x$, which has two orders of magnitude lower electrical conductivity than these metals, shows EMI SE values similar to those of metals (tables S2 and S3). For comparison, thermally reduced graphene oxide film (8.4 μm) that possessed lower electrical conductivity is also plotted and fell far below the other materials (*32*).

The massive EMI SE of MXene can be understood from several proposed mechanisms shown in Fig. 4B. The EMI shielding originates from the excellent electrical conductivity of MXene and partially from the layered architecture of the films. A potential mechanism can be explained as follows: As EMWs strike the surface of a MXene flake, some EM waves are immediately reflected because of abundant free electrons at the surface of the highly conductive MXene (*9*, *10*). The remaining waves pass through the MXene lattice structure where interaction with the high electron density of MXene induces currents that contribute to ohmic losses, resulting in a drop in energy of the EMWs. The surviving EMWs, after passing through the first layer of $Ti_3C_2T_x$ (marked as "I" in Fig. 4B), encounter the next barrier layer (marked as "II"), and the phenomenon of EMW attenuation repeats. Simultaneously, layer II acts as a

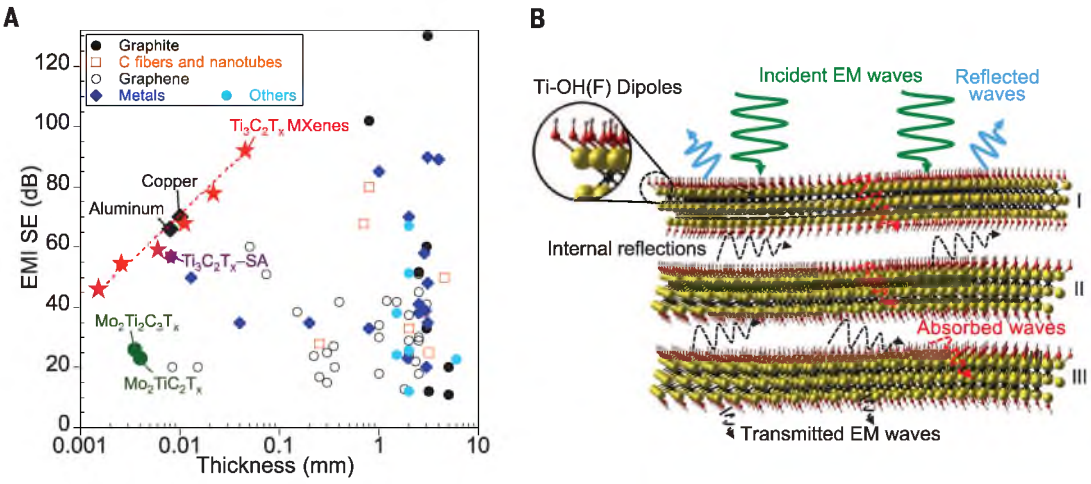

Fig. 4. Comparison of EMI SE with the previous literature and shielding mechanisms. (**A**) EMI SE versus thickness of different materials. Each symbol indicates a set of material category as follows: $Ti_3C_2T_x$ MXenes (red star), $Ti_3C_2T_x$-SA composite (purple star), molybdenum MXenes (green filled circle), copper and aluminum foils (black diamond), metals (blue diamond), graphene (open circle), carbon fibers and nanotubes (open square), graphite (black filled circle), other materials (blue filled circle). A detailed description of each data point is presented in table S2. (**B**) Proposed EMI shielding mechanism. Incoming EM waves (green arrows) strike the surface of a MXene flake. Because reflection occurs before absorption, part of the EM waves is immediately reflected from the surface owing to a large number of charge carriers from the highly conducting surface (light blue arrows), whereas induced local dipoles, resulting from termination groups, help with absorption of the incident waves passing through the MXene structure (dashed blue arrows). Transmitted waves with less energy are then subjected to the same process when they encounter the next MXene flake, giving rise to multiple internal reflections (dashed black arrows), as well as more absorption. Each time an EM wave is transmitted through a MXene flake, its intensity is substantially decreased, resulting in an overall attenuated or completely eliminated EM wave.

reflecting surface and gives rise to multiple internal reflections. The EMWs can be reflected back and forth between the layers (I, II, III, and so on) until completely absorbed in the structure. This is in marked contrast to pure metals that have a regular crystallographic structure and no interlayer reflecting surface available to provide the internal multiple reflection phenomenon. Thus, the nacre-like (or laminated) structure provides MXene with the ability to behave as a multilevel shield. The SEM image (Fig. 2C) shows well-aligned MXene layers in both pure $Ti_3C_2T_x$ and its composites. Considering a 45-μm-thick $Ti_3C_2T_x$ film, thousands of 2D $Ti_3C_2T_x$ sheets act as barriers to EMWs. As the overall EMI value goes above 15 dB, it is generally assumed that the contribution from internal reflections is minimal (*1*). However, in the layered structure of MXenes, multiple internal reflections cannot be ignored. The multiple reflection effect, nevertheless, is included with absorption because the re-reflected waves get absorbed or dissipated in the form of heat within the material (*8*, *9*, *27*). Furthermore, MXene flake surface terminations may play a role as well. Local dipoles between Ti and terminating groups (–F, =O, or –OH) may be created when subjected to an alternating electromagnetic field. Fluorine, in particular, being highly electronegative, can induce this kind of dipole polarization. The ability of each element to interact with incoming EMWs leads to polarization losses, which in turn improve the overall shielding.

We have shown here that flexible $Ti_3C_2T_x$ films with thicknesses ranging from 1 to 45 μm exhibit excellent electrical conductivity and EMI shielding capabilities. The reported EMI SE values are the highest of any known synthetic materials with similar thickness. Moreover, excellent shielding ability is maintained after adding SA to create polymer composite films. This allows the use of very thin films for device shielding to help eliminate EM radiation as miniaturization of electronics progresses. This study is set to pave the way for a large family of 2D materials that are far superior in performance compared to currently used materials in EMI shielding applications. The 2D structure, combined with high electrical conductivity and good electronic coupling between the layers, is responsible for the extremely high EMI shielding efficiency of MXenes.

REFERENCES AND NOTES

1. Z. Chen, C. Xu, C. Ma, W. Ren, H. M. Cheng, *Adv. Mater.* **25**, 1296–1300 (2013).
2. D. X. Yan *et al.*, *Adv. Funct. Mater.* **25**, 559–566 (2015).
3. N. Yousefi *et al.*, *Adv. Mater.* **26**, 5480–5487 (2014).
4. Y. Zhang *et al.*, *Adv. Mater.* **27**, 2049–2053 (2015).
5. A. H. Frey, *Environ. Health Perspect.* **106**, 101–103 (1998).
6. D. D. L. Chung, *Carbon* **39**, 279–285 (2001).
7. N. C. Das *et al.*, *Polym. Eng. Sci.* **49**, 1627–1634 (2009).
8. M. H. Al-Saleh, W. H. Saadeh, U. Sundararaj, *Carbon* **60**, 146–156 (2013).
9. H. B. Zhang, Q. Yan, W. G. Zheng, Z. He, Z. Z. Yu, *ACS Appl. Mater. Interfaces* **3**, 918–924 (2011).
10. J.-M. Thomassin *et al.*, *Mater. Sci. Eng. Rep.* **74**, 211–232 (2013).
11. M.-S. Cao, X.-X. Wang, W.-Q. Cao, J. Yuan, *J. Mater. Chem. C* **3**, 6589–6599 (2015).
12. M. Naguib, V. N. Mochalin, M. W. Barsoum, Y. Gogotsi, *Adv. Mater.* **26**, 992–1005 (2014).
13. M. R. Lukatskaya *et al.*, *Science* **341**, 1502–1505 (2013).
14. B. Anasori *et al.*, *ACS Nano* **9**, 9507–9516 (2015).
15. J. Halim *et al.*, *Adv. Funct. Mater.* **26**, 3118–3127 (2016).
16. Z. Ling *et al.*, *Proc. Natl. Acad. Sci. U.S.A.* **111**, 16676–16681 (2014).
17. M. Boota *et al.*, *Adv. Mater.* **28**, 1517–1522 (2016).
18. I. Kovalenko *et al.*, *Science* **334**, 75–79 (2011).
19. B. Anasori *et al.*, *Nanoscale Horizons* **1**, 227–234 (2016).
20. M. Khazaei *et al.*, *Adv. Funct. Mater.* **23**, 2185–2192 (2013).
21. J. J. Liang *et al.*, *Carbon* **47**, 922–925 (2009).
22. F. Shahzad, P. Kumar, Y.-H. Kim, S. M. Hong, C. M. Koo, *ACS Appl. Mater. Interfaces* **8**, 9361–9369 (2016).
23. Z. Zeng *et al.*, *Carbon* **96**, 768–777 (2016).
24. S. Varshney, A. Ohlan, V. K. Jain, V. P. Dutta, S. K. Dhawan, *Ind. Eng. Chem. Res.* **53**, 14282–14290 (2014).
25. P. Xu *et al.*, *J. Phys. Chem. B* **112**, 2775–2781 (2008).
26. L. Liu *et al.*, *J. Magn. Magn. Mater.* **324**, 1786–1790 (2012).
27. A. Ameli, M. Nofar, S. Wang, C. B. Park, *ACS Appl. Mater. Interfaces* **6**, 11091–11100 (2014).
28. B. Shen, Y. Li, W. Zhai, W. Zheng, *ACS Appl. Mater. Interfaces* **8**, 8050–8057 (2016).
29. Y. Yang, M. C. Gupta, K. L. Dudley, R. W. Lawrence, *Nano Lett.* **5**, 2131–2134 (2005).
30. Y. Chen *et al.*, *Adv. Funct. Mater.* **26**, 447–455 (2016).
31. Z. Zeng *et al.*, *Adv. Funct. Mater.* **26**, 303–310 (2016).
32. B. Shen, W. Zhai, W. Zheng, *Adv. Funct. Mater.* **24**, 4542–4548 (2014).

ACKNOWLEDGMENTS

This work was supported in part by the U.S. National Science Foundation under grant DMR-1310245. F.S., M.A., C.B.H., B.A., S.M.H., C.M.K., and Y.G. are inventors on patent application 62/326,074 submitted by Drexel University that covers MXene films and composites for EMI shielding. M.A. was supported by the Libyan North America Scholarship Program funded by the Libyan Ministry of Higher Education and Scientific Research. This work was also supported by the Fundamental R&D Program for Core Technology of Materials and the Industrial Strategic Technology Development Program funded by the Ministry of Trade, Industry and Energy, and the Disaster and Safety Management Institute by the Ministry of Public Safety and Security of Korean Government, Republic of Korea, and partially by the Korea Institute of Science and Technology.

SUPPLEMENTARY MATERIALS

www.sciencemag.org/content/353/6304/1137/suppl/DC1
Materials and Methods
Supplementary Text
Figs. S1 to S6
Tables S1 to S3
References (*33*–*112*)

29 May 2016; accepted 10 August 2016
10.1126/science.aag2421

Electromagnetic interference shielding with 2D transition metal carbides (MXenes)

Faisal Shahzad, Mohamed Alhabeb, Christine B. Hatter, Babak Anasori, Soon Man Hong, Chong Min Koo and Yury Gogotsi

Science **353** (6304), 1137-1140.
DOI: 10.1126/science.aag2421